LAWRENCE
LIVERMORE
NATIONAL
LABORATORY

LLNL-JRNL-461792

S-matrix Calculations of Energy Levels of the Lithium Isoelectronic Sequence

J. sapirstein, K. T. Cheng

November 8, 2010

Physical Review A

Disclaimer

S-matrix calculations of energy levels of the lithium isoelectronic sequence

J. Sapirstein*

Department of Physics, University of Notre Dame, Notre Dame, IN 46556

K. T. Cheng (鄭國錚)†

Lawrence Livermore National Laboratory, Livermore, CA 94550

(Dated: November 1, 2010)

Abstract

A QED approach to the calculation of the spectra of the lithium isoelectronic sequence is implemented. A modified Furry representation based on the Kohn-Sham potential is used to evaluate all one- and two-photon diagrams with the exception of the two-loop Lamb shift. Three-photon diagrams are estimated with Hamiltonian methods. After incorporating recent calculations of the two-loop Lamb shift and recoil corrections a comprehensive tabulation of the $2s$, $2p_{1/2}$ and $2p_{3/2}$ energy levels as well as the $2s-2p_{1/2}$ and $2s-2p_{3/2}$ transition energies for $Z=10-100$ is presented.

PACS numbers: 12.20.Ds, 31.20.Tz, 31.30.Jv

*jsapirst@nd.edu

†ktcheng@llnl.gov

I. INTRODUCTION

The many-body problem in atoms and ions is most often treated in a Hamiltonian formalism. As a starting point the many-electron Schrödinger equation, or a relativistic extension of it, is treated with many-body perturbation theory (MBPT) [1], and quantum electrodynamic (QED) corrections are then included as perturbations. An example of the first part of this approach is the MBPT treatment of the lithiumlike [2] and sodiumlike [3] isoelectronic sequences, where a Hartree-Fock potential is taken as a starting point of a perturbation expansion that includes Coulomb interactions through third order, instantaneous Breit interactions through second order, and the effect of retardation on the Breit interaction in lowest order. In these early works discrepancies with experiment were used to infer the QED corrections, but since then the direct calculation of the one-loop Lamb shift has been carried out [4], and the bulk of the discrepancy is removed when the one-loop Lamb shift is added to the MBPT results.

While this approach is successful in accounting for the spectra of the above mentioned sequences at the few tenths of an eV level, subtle effects relating to retardation and negative energy states begin to be important when levels under 0.1 eV are reached in modern experiments for high-Z ions [5–7]. It is rather complicated to restore the effect of negative energy states, which are usually omitted from Hamiltonian treatments in order to avoid the continuum dissolution problem [8], and in addition the treatment of retardation is problematical [9]. These issues can be avoided altogether if the Hamiltonian formalism is simply abandoned, and replaced with the Feynman diagram oriented approach offered by S-matrix theory [10], which will be used here, or the essentially equivalent Green's function techniques used by the St. Petersburg group [11].

The application of either QED-based theory to highly-charged ions is analogous to the QED treatment of the electron anomalous magnetic moment, where evaluation of a limited, unambiguous set of Feynman diagrams accounts for all relevant physics up to a given precision governed by powers of the fine structure constant α. For highly-charged many-electron ions, the relevant expansion parameter is the number of virtual photons in the Feynman diagrams, with factors of α or $1/Z$ providing strong suppression of diagrams with three or more photons. For this reason, only the relatively few diagrams involving one or two photons need to be treated, although weak-field expansion in the parameter $Z\alpha$, which simplifies the treat-

ment of light systems, is not suitable for high-Z ions and bound state electron propagators have to be used. Residual contributions from the large number of three-photon graphs have not yet been calculated with QED methods. They are dominated by correlation diagrams involving photon exchanges between different electrons, and, as will be discussed below, can be approximated by using the Hamiltonian method described in the first paragraph. This QED approach has been implemented for highly-charged lithiumlike ions in Refs. [11] and [12]. The latter paper concentrated on a single transition energy, the $2s - 2p_{3/2}$ splitting for lithiumlike bismuth, and used basis set techniques to evaluate two-photon exchange diagrams. In this paper, we replace the basis set techniques with differential equation methods and give a complete treatment of the $2s$, $2p_{1/2}$ and $2p_{3/2}$ energy levels as well as the $2s-2p_{1/2}$ and $2s - 2p_{3/2}$ transition energies along the isoelectronic sequence.

Three additional theoretical issues enter when high precision is required. The first has to do with the finite mass of the nucleus, which leads to recoil corrections. While suppressed by a factor of m/M, where m is the electron mass and M the mass of the nucleus, these corrections, which are highly nontrivial to calculate, must be included. The second issue is higher-order contributions to the Lamb shift, specifically the two-loop Lamb shift. This effect is sufficiently large at high Z that its value was inferred in Ref. [12] for lithiumlike bismuth, but, as with the one-loop Lamb shift, it can now be calculated directly [13, 14]. Finally, the polarizability of some nuclei is large enough that a small but non-negligible effect results. These nuclear polarization corrections have been studied for the $n = 2$ states of heavy lithiumlike ions [15] and will be included in the present ionization and transition energies.

In our previous work [12] we showed that essentially identical results were obtained regardless of the model potential used to define the QED representation. Here we specialize to the Kohn-Sham potential [16], a self-consistent local potential similar to the Dirac-Fock potential. In the next section, the S-matrix formalism is described, and the Kohn-Sham potential defined. In Sec. III, one-photon diagrams are treated. In Sec. IV, two-photon diagrams, with the exception of the two-loop Lamb shift, are evaluated. In Sec. V, the smaller corrections from three-photon diagrams, nuclear recoil, two-loop Lamb shift and nuclear polarization are discussed. The main result of the paper is a comprehensive tabulation of the ionization potentials of the $2s$, $2p_{1/2}$, and $2p_{3/2}$ states for $Z = 10 - 100$, along with the $2s - 2p_{1/2}$ and $2s - 2p_{3/2}$ transition energies. For the sake of brevity, only the complete

theoretical result is presented for the isoelectronic series, but to illustrate the importance of the various corrections, the breakdown of contributions for a few ions along the isoelectronic sequence will be given in a separate table. A discussion of the comparison of the present theory with experiment and other calculations, along with directions for future progress, is given in the concluding section.

II. S-MATRIX FORMULATION

S-matrix calculations [10] of atomic structure use the fact that energy levels of an atom can be related to matrix elements of an operator that evolves the atom from $t = -\infty$ to $t = \infty$,

$$S_{\epsilon,\lambda} = T\Big(e^{-i\lambda \int dt e^{-\epsilon|t|} H_I(t)}\Big), \tag{1}$$

through $E = E_0 + \Delta E$, where

$$\Delta E = \lim_{\epsilon \to 0} \frac{i\epsilon}{2} \lim_{\lambda \to 1} \frac{\partial}{\partial \lambda} \ln \langle \Phi_0 | S_{\epsilon,\lambda} | \Phi_0 \rangle. \tag{2}$$

Here E_0 is the energy of the atom at times $t = \pm\infty$, where the interaction Hamiltonian, defined below, is suppressed by the adiabatic damping factor ϵ. For the isoelectronic sequence we will be treating here, the state $|\Phi_0\rangle$ can be represented in a manner identical to that used in MBPT,

$$|\Phi_0\rangle = a_v^\dagger \, |0_{\rm c}\rangle, \tag{3}$$

where v represents a valence electron and $|0_{\rm c}\rangle$ a filled heliumlike core. The wave functions are defined by the interaction representation chosen to define H_I, and obey the Dirac equation in a spherically symmetric potential $U(r)$,

$$\left[\vec{\alpha} \cdot \vec{p} + \beta m + U(r)\right] \psi_n(\vec{x}) = \epsilon_n \psi_n(\vec{x}), \tag{4}$$

where $r = |\vec{x}|$. Natural units in which $\hbar = c = 1$ are used in this work unless otherwise specified. The lowest-order energy $E^{(0)}$ is given by

$$E^{(0)} = \epsilon_v + 2\epsilon_a, \tag{5}$$

where a represents the $1s_{1/2}$ core state. The second term in the above formula for $E^{(0)}$, which does not contribute either to valence ionization or transition energies, will be suppressed in

the following, and this convention will be followed for the higher-order corrections considered in this paper.

While there are sufficiently few electrons in lithiumlike ions that reasonable results can be obtained starting from the Coulomb potential

$$U_{\rm C}(r) = -\frac{Z_{\rm nuc}(r)\alpha}{r}\,, \tag{6}$$

we instead choose to incorporate some screening by using the Kohn-Sham potential [16] defined by

$$U_{\rm KS}(r) = U_{\rm C}(r) + \alpha\int dr'\,\frac{1}{r_>}\rho_t(r') - \frac{2}{3}\left[\frac{81}{32\pi^2}\,r\rho_t(r)\right]^{1/3}\frac{\alpha}{r}\,, \tag{7}$$

where

$$\rho_t(r) = g_v^2(r) + f_v^2(r) + 2\left[g_a^2(r) + f_a^2(r)\right]. \tag{8}$$

Here $g(r)$ and $f(r)$ are the upper and lower components of Dirac wave functions self-consistently determined, v is the $2s$ valence electron, and $Z_{\rm nuc}(r)$ accounts for the finite size of the nucleus using a Fermi distribution with parameters taken from [17], except for thorium and uranium where the c parameters are changed from 6.9264 and 6.9868 fm in [17] to 7.0598 and 7.13753 fm as deduced from measurements [18, 19]. A related potential that will arise in the treatment of screening of the Lamb shift is the core-Hartree (CH) potential defined by

$$U_{\rm CH}(r) = U_{\rm C}(r) + \alpha\int dr'\,\frac{1}{r_>}\rho_c(r') \tag{9}$$

with

$$\rho_c(r) = 2\left[g_a^2(r) + f_a^2(r)\right]. \tag{10}$$

Neglecting core energies, the binding energies ϵ_v associated with the Kohn-Sham potential are shown as $E^{(0)}$ for a few lithiumlike ions in Table I.

When dealing with free-electron processes, the most appropriate treatment of QED is the interaction representation, which is a unitary transformation that subtracts the free-electron Hamiltonian H_0 from the full Hamiltonian. Early applications of QED to the bound state problem were primarily concerned with hydrogen and employed a different kind of interaction representation known as the Furry representation [20] in which the interaction of the electron with the Coulomb field of the nucleus is also kept in H_0. Specifically, the transformation from a Schrödinger picture wave function $|\Psi_S\rangle$ to a Furry picture wave function $|\Psi_I\rangle$ is

$$|\Psi_I\rangle = e^{iH_0t}|\Psi_S\rangle, \tag{11}$$

where

$$H_0 = \int d^3x\, \psi^\dagger(\vec{x},t)\,[\vec{\alpha}\cdot\vec{p} + \beta m + U_{\rm C}(r)]\,\psi(\vec{x},t), \tag{12}$$

and the interaction Hamiltonian is defined as

$$H_I(t) = e\int d^3x\, \bar{\psi}(\vec{x},t)\gamma_\mu A^\mu(\vec{x},t)\psi(\vec{x},t), \tag{13}$$

with normal ordering understood. This formalism applies equally well to the case when the Coulomb potential $U_{\rm C}(r)$ in Eq. (12) is replaced with a non-Coulomb local potential $U(r)$, chosen here to be $U_{\rm KS}(r)$, providing that a *counter-potential* term is added to the interaction Hamiltonian,

$$\delta H_I(t) = \int d^3x\, \psi^\dagger(\vec{x},t)\,[U_{\rm C}(r) - U(r)]\,\psi(\vec{x},t). \tag{14}$$

When the field operators in the above are replaced with specific wave functions, we encounter the frequently occuring matrix element

$$\tilde{U}_{ij} \equiv \int d^3x\, \psi_i^\dagger(\vec{x})\,\tilde{U}(r)\,\psi_j(\vec{x}), \tag{15}$$

where $\tilde{U}(r) \equiv U_{\rm C}(r) - U(r) = U_{\rm C}(r) - U_{\rm KS}(r)$ here. In this paper we will be concerned with terms up to fourth order in $H_I(t)$ and second order in $\delta H_I(t)$, which correspond to Feynman diagrams with up to two virtual photons.

III. ONE-PHOTON PHYSICS

The diagrams involving one photon are shown in Fig. 1. If we define the matrix element

$$g_{ijkl}(E) = \alpha\int d^3x\, d^3y\, \frac{e^{iE|\vec{x}-\vec{y}|}}{|\vec{x}-\vec{y}|}\,\bar{\psi}_i(\vec{x})\gamma^\mu\psi_k(\vec{x})\,\bar{\psi}_j(\vec{y})\gamma_\mu\psi_l(\vec{y}), \tag{16}$$

the one-photon exchange term of Fig. 1a and the counter-potential term of Fig. 1b give the energy shift

$$E^{(1)} = \sum_a [(g_{avav}(0) - g_{avva}(E_{va})] - \tilde{U}_{vv}, \tag{17}$$

where $E_{va} = \epsilon_v - \epsilon_a$. This part of one-photon physics we refer to as *structure*-related, as we will do with any diagram that has, as a limit, an expression from MBPT. Specifically, while we work in the Feynman gauge, were we to work in the Coulomb gauge, the Coulomb photon part of $E^{(1)}$ would exactly reproduce first-order MBPT results when only Coulomb interactions are included. We note here that because we use a local potential, gauge invariance

ensures that a complete Coulomb gauge calculation, including retarded transverse-photon exchange, would reproduce the results of the present Feynman gauge calculation. The contributions of $E^{(1)}$ are given in Table I. We present only its real part, but note that an imaginary part, related to the decay rate of the ion, is also in general present. While this plays no role in one-photon exchange, it will play a role in the two-photon calculations described below.

More difficult to evaluate are the radiative diagrams of Figs. 1c and 1d for the one-loop vacuum-polarization and self-energy, respectively. The vacuum polarization term in the Uehling approximation is given by

$$E_{\rm Uel}^{\rm VP} = \frac{\alpha^2}{4\pi^2}\int_0^1 dy\,\frac{y^2(1-y^2/3)}{1-y^2}\int d^3x\,\psi_v^\dagger(\vec{x})\psi_v(\vec{x})\int d^3r\,\frac{e^{-\frac{2m|\vec{x}-\vec{r}|}{\sqrt{1-y^2}}}}{|\vec{x}-\vec{r}|}\,\vec{\nabla}_r^2\left(\frac{Z_{\rm eff}(r)}{r}\right), \tag{18}$$

where $Z_{\rm eff}(r) = -r\,U_{\rm KS}(r)/\alpha$ is the effective charge for the Kohn-Sham potential. In addition, Wichmann-Kroll [21] corrections $E_{\rm WK}^{\rm VP}$, must be added. We have developed techniques for the evaluation of both parts of the vacuum polarization calculation. The Wichmann-Kroll part of the calculation, in particular, is similar to the self-energy calculation and involves partial wave expansions in configuration space using numerical bound-state Green's functions. Our method has been described in Ref. [22]. The present vacuum polarization results are shown as "Uehling" and "WK" in Table I.

The self-energy (SE) can be written as $E_{1\gamma}^{\rm SE} = \Sigma_{vv}(\epsilon_v)$, where

$$\Sigma_{jl}(\epsilon) \equiv -ie^2\int d^3x\int d^3y\int\frac{d^nk}{(2\pi)^n}\,\frac{e^{i\vec{k}\cdot(\vec{x}-\vec{y})}}{k^2+i\delta}\,\bar{\psi}_j(\vec{x})\gamma_\mu S_F(\vec{x},\vec{y};\epsilon-k_0)\gamma^\mu\psi_l(\vec{y}), \tag{19}$$

and the self-mass counterterm is understood to be included. In the above, $n = 4-\epsilon$ is used to regulate the integral over k, and after renormalization the limit $\epsilon \to 0$ is taken. Here, self-energies are calculated non-perturbatively to all orders of $Z\alpha$ with partial wave expansions in configuration space using numerical bound-state Green's functions. Subtraction terms involving the free-electron propagator are evaluated in momentum space with Fourier-transformed wave functions. Details of these calculations, with references to earlier works, can be found in [23]. As mentioned above, we do not consider the self-energies of the core states, but note that they enter into the two-photon calculation. As with one-photon exchange, imaginary parts are generally present, and play a role in the two-photon calculation. The real parts of the self-energies are presented as "SE" in Table I.

IV. TWO-PHOTON PHYSICS

A. Structure diagrams

We begin our discussion of two-photon physics with correlation diagrams in which there is only one electron propagator between two virtual photons that are exchanged among three different electrons (Fig. 2a), between a virtual photon and a counter-potential (Fig. 2b) and between two counter-potentials (Fig. 2c). Since we omit diagrams in which the photons interact with only core electrons, there will always be one valence electron v and up to two core electrons a and b. Defining $E_{ij} = \epsilon_i - \epsilon_j$, we find

$$\begin{aligned}
\Delta E_{2\gamma} \;=\; & \sum_{abi}^{i\neq v} \frac{[g_{bvbi}(0) - g_{vbbi}(E_{vb})]\,[g_{iava}(0) - g_{iaav}(E_{va})]}{\epsilon_v - \epsilon_i} \\
& + \sum_{abi}^{i\neq a} \frac{[g_{vavi}(0) - g_{vaiv}(-E_{va})]\,[g_{ibab}(0) - g_{ibba}(E_{ab})]}{\epsilon_a - \epsilon_i} \\
& + \sum_{abi}^{i\neq a} \frac{[g_{viva}(0) - g_{ivva}(-E_{va})]\,[g_{abib}(0) - g_{abbi}(E_{ab})]}{\epsilon_a - \epsilon_i} \\
& - \sum_{abi} \frac{[g_{avbi}(E_{ab}) - g_{avib}(E_{vb})]\,[g_{ibva}(E_{ab}) - g_{ibav}(E_{vb})]}{\epsilon_a + \epsilon_v - \epsilon_i - \epsilon_b} \\
& + \sum_{abi} \frac{[g_{bavi}(-E_{vb}) - g_{abvi}(-E_{va})]g_{ivba}(-E_{av})}{\epsilon_a + \epsilon_b - \epsilon_v - \epsilon_i} \\
& - \sum_{ai}^{i\neq v} \frac{[g_{avai}(0) - g_{vaai}(E_{va})]\,\tilde{U}_{iv} + \tilde{U}_{vi}\,[g_{aiav}(0) - g_{iaav}(E_{av})]}{\epsilon_v - \epsilon_i} \\
& - \sum_{ai}^{i\neq a} \frac{[g_{aviv}(0) - g_{vaiv}(-E_{va})]\,\tilde{U}_{ia} + \tilde{U}_{ai}\,[g_{ivav}(0) - g_{ivva}(-E_{va})]}{\epsilon_a - \epsilon_i} \\
& + \sum_{i}^{i\neq v} \frac{\tilde{U}_{vi}\,\tilde{U}_{iv}}{\epsilon_v - \epsilon_i}\,.
\end{aligned} \tag{20}$$

Note that the sign of E in $g_{ijkl}(E)$ is significant. Furthermore, there is a second kind of contribution coming from these graphs known as derivative terms, which are sensitive to that sign. They are associated with the $i = v$ and $i = a$ terms excluded in the above equation and are given by

$$\begin{aligned}
\Delta E'_{2\gamma} \;=\; & \sum_{ab} g'_{avvb}(E_{va})[g_{vbva}(0) - g_{vbav}(E_{va})] - \sum_{ab} g'_{vbav}(-E_{va})[g_{vaba}(0) - g_{vaab}(0)] \\
& - \sum_{ab} g'_{vbbv}(E_{va})[g_{vava}(0) - g_{vaav}(E_{va})] \\
& + \tilde{U}_{vv} \sum_{a} g'_{vaav}(E_{va}) + \tilde{U}_{aa} \sum_{a} g'_{vaav}(-E_{va}).
\end{aligned} \tag{21}$$

The second structure-related class of two-photon diagrams are shown in Figs. 2d and 2e, which we refer to as the ladder (L) and crossed-ladder (X) diagrams respectively. They give the energy shifts

$$\Delta E_L = \frac{i}{2\pi} \sum_{aij} \int_{-\infty}^{\infty} dz \, \frac{g_{ijav}(z)[g_{avij}(z) - g_{avji}(z - E_{va})]}{[\epsilon_a + z - \epsilon_i(1 - i\delta)]\,[\epsilon_v - z - \epsilon_j(1 - i\delta)]} \tag{22}$$

and

$$\Delta E_X = \frac{i}{2\pi} \sum_{aij} \int_{-\infty}^{\infty} dz \left\{ \frac{g_{ajiv}(z) g_{ivaj}(z)}{[\epsilon_a + z - \epsilon_i(1 - i\delta)]\,[\epsilon_v + z - \epsilon_j(1 - i\delta)]} - \frac{g_{ajia}(z) g_{ivvj}(z - E_{va})}{[\epsilon_a + z - \epsilon_i(1 - i\delta)]\,[\epsilon_a + z - \epsilon_j(1 - i\delta)]} \right\}. \tag{23}$$

The analysis of these diagrams, which are structure-related inasmuch as they include contributions to the second-order MBPT result, is complicated, but parallels the treatment of the ladder and crossed ladder for excited states in helium [24], where more details can be found. The most computationally intensive part of the evaluation of these diagrams involves the z integration. A Wick rotation $z \to i\omega$ leads to terms in which the contour surrounds poles or photon cuts plus the ω integral, which is evaluated with Gaussian integration. If done with finite basis sets, considerable computational time is needed even when the partial wave expansion of the propagators is relatively limited. To avoid this problem, we use differential equation techniques instead. When using this method, the relative magnitudes of the four position vectors involved must be considered, which leads to 24 regions for each diagram ($x < y < z < w$, $y < x < z < w$, etc.). While this entails more coding than that required for finite basis sets, the resulting programs run far more quickly, and allow us to extend the partial wave expansion to $l = 20$. Use of this form of the propagator encounters one complication of note, which involves the fact that certain intermediate states must be excluded. As differential equation techniques implicitly include all intermediate states, they lead to linear divergences in two of the diagrams, the ladder direct and crossed-ladder direct. It can be shown, however, that the excluded states that cancel these divergences are equal and opposite in sign, so we simply combine these terms to obtain a finite answer. The result still includes certain finite terms coming from states that should be excluded, but these are simply evaluated independently and subtracted.

The sum of the two-photon structure diagrams is denoted $E^{(2)}$ in Table I. It is notable that this rather involved set of calculations gives a result quite close to the MBPT procedure

of Ref. [2], even though MBPT excludes contributions from the negative energy states and its treatment of retardation is less complete than the present approach. However, small differences that are important at the level of the most precise experiments do exist. An important example involves the $2s - 2p_{3/2}$ transition energy of lithiumlike bismuth, where the inference of the two-loop Lamb shift requires a QED approach [12]. Specifically, the Hamiltonian method described in the Introduction contributes 0.174 eV in second order. While this calculation is part of the complete QED calculation, from Table I we see a very different $E^{(2)}$ result of 0.052 eV. The difference of 0.122 eV is relatively small compared to most experimental uncertainties, but the high-precision EBIT measurement [5] for lithiumlike bismuth, which has achieved an accuracy of 0.039 eV, makes it important. In particular, since this difference is about the same size as the two-loop Lamb shift but of the opposite sign, were MBPT to be used and combined with an accurate screened Lamb shift calculation, agreement with experiment would have been found, and the two-loop Lamb shift would have been inferred to be negligible. Use of the correct treatment of the structure term in Ref. [12], however, led to a discrepancy of 0.175 eV, which was identified as due mainly to the two-loop Lamb shift, a finding subsequently confirmed by the St. Petersburg group [13, 14] with direct calculations.

B. Lamb shift screening diagrams

Excluding two-loop Lamb shift, the two-photon diagrams that involve radiative corrections are shown in Figs. 3 and 4. We have in a previous paper [22] described the evaluation of screening corrections to vacuum polarization, depicted in Fig. 3, and shall refer details of these calculations to that work. The treatment of screening of the self-energy requires the evaluation of the graphs of Fig. 4. We begin with Figs. 4a and 4b in which a self-energy diagram is present with an exchanged photon or a counter-potential to one side. When the intermediate propagator is represented as a spectral decomposition and has no states degenerate with the core or valence states, the effect of these diagrams can be treated as self-energy diagrams with one state replaced with a perturbed orbital, and we have the contributions

$$\Sigma^{\mathrm{PO}} = \Sigma_{v\tilde{v}} + \Sigma_{\tilde{v}v} + \sum_a (\Sigma_{a\tilde{a}} + \Sigma_{\tilde{a}a}), \tag{24}$$

where

$$\psi_{\tilde{v}}(\vec{y}) \equiv \alpha \sum_{m\neq v,a} \int \frac{d^3z\, d^3w}{|\vec{z}-\vec{w}|} \frac{\psi_m(\vec{y})}{\epsilon_v-\epsilon_m} \Big[\bar{\psi}_m(\vec{z})\gamma_\mu\psi_v(\vec{z})\,\bar{\psi}_a(\vec{w})\gamma^\mu\psi_a(\vec{w}) - e^{iE_{va}|\vec{z}-\vec{w}|}\,\bar{\psi}_m(\vec{z})\gamma_\mu\psi_a(\vec{z})\,\bar{\psi}_a(\vec{w})\gamma^\mu\psi_v(\vec{w})\Big] - \sum_{m\neq v}\int d^3z\,\frac{\psi_m(\vec{y})}{\epsilon_v-\epsilon_m}\,\psi_m^\dagger(\vec{z})\tilde{U}(z)\psi_v(\vec{z}) \tag{25}$$

is a valence orbital perturbed either by the exchange of a photon with the core electrons or else by the counter potential $\tilde{U}(z)$, and

$$\psi_{\tilde{a}}(\vec{y}) \equiv \alpha \sum_{m\neq a}^{\kappa_m=\kappa_a} \int \frac{d^3z\, d^3w}{|\vec{z}-\vec{w}|} \frac{\psi_m(\vec{y})}{\epsilon_a-\epsilon_m} \Big[\bar{\psi}_m(\vec{z})\gamma_\mu\psi_a(\vec{z})\,\bar{\psi}_v(\vec{w})\gamma^\mu\psi_v(\vec{w}) - e^{iE_{va}|\vec{z}-\vec{w}|}\,\bar{\psi}_m(\vec{z})\gamma_\mu\psi_v(\vec{z})\,\bar{\psi}_v(\vec{w})\gamma^\mu\psi_a(\vec{w})\Big] \tag{26}$$

is a core orbital perturbed by the exchange of a photon with the valence electron.

When there is a degeneracy, derivative terms arise in which either the energy dependence of the self-energy function or the one-photon exchange part of the diagram gets differentiated. This leads to a single expression for the *valence* derivative term,

$$E_{der}(v) = E_v^{(1)}\Sigma'_{vv}(\epsilon_v) - \sum_a g'_{vaav}(E_{va})\Sigma_{vv}(\epsilon_v), \tag{27}$$

and a set of *core* derivative terms,

$$E_{der}(a) = \Sigma'_{aa}\sum_a [g_{vava}(0) - g_{avva}(-E_{va})] - \Sigma_{aa}\sum_a g'_{avva}(-E_{va}). \tag{28}$$

These derivative terms have ultraviolet divergent parts that cancel with the vertex diagrams discussed below. The ultraviolet divergent part comes from the part of the electron propagator when it is free, so this term is treated separately. The remaining term, where the full propagator has the free propagator subtracted to form an ultraviolet finite quantity, breaks into two terms upon the Wick rotation $k_0 \to i\omega$, one in which the ω integration is carried out numerically, and one in which double poles are encircled during the Wick rotation, which leads to a derivative term. The ω integration has singularities at small ω that we regulate through the device of taking $\epsilon_v \to \epsilon_v(1-\delta)$ and $\epsilon_a \to \epsilon_a(1-\delta)$. The resulting integrals have a $\ln(\delta)$ dependence that cancels similar behavior present in the vertex diagrams discussed below.

We now treat the two vertex diagrams of Figs. 4c and 4d, calling the contributions ΔE_i, $i = 1 - 5$, where

$$\begin{aligned}\Delta E_1 &= -4i\pi\alpha^2 \sum_a \int d^3x\, d^3y\, d^3z\, d^3w\, \frac{1}{|\vec{y}-\vec{w}|} \int \frac{d^nk}{(2\pi)^n} \frac{e^{i\vec{k}\cdot(\vec{x}-\vec{z})}}{k^2}\, \bar{\psi}_v(\vec{x})\gamma_\mu \\ &\quad \times S_F(\vec{x},\vec{y};\epsilon_v - k_0)\gamma_\nu S_F(\vec{y},\vec{z};\epsilon_v - k_0)\gamma^\mu \psi_v(\vec{z})\bar{\psi}_a(\vec{w})\gamma^\nu \psi_a(\vec{w}), \qquad (29)\end{aligned}$$

$$\begin{aligned}\Delta E_2 &= 4i\pi\alpha^2 \sum_a \int d^3x\, d^3y\, d^3z\, d^3w\, \frac{e^{iE_{va}|\vec{y}-\vec{w}|}}{|\vec{y}-\vec{w}|} \int \frac{d^nk}{(2\pi)^n} \frac{e^{i\vec{k}\cdot(\vec{x}-\vec{z})}}{k^2}\, \bar{\psi}_v(\vec{x})\gamma_\mu \\ &\quad \times S_F(\vec{x},\vec{y};\epsilon_v - k_0)\gamma_\nu S_F(\vec{y},\vec{z};\epsilon_a - k_0)\gamma^\mu \psi_a(\vec{z})\bar{\psi}_a(\vec{w})\gamma^\nu \psi_v(\vec{w}), \qquad (30)\end{aligned}$$

$$\begin{aligned}\Delta E_3 &= -4i\pi\alpha^2 \sum_a \int d^3x\, d^3y\, d^3z\, d^3w\, \frac{1}{|\vec{y}-\vec{w}|} \int \frac{d^nk}{(2\pi)^n} \frac{e^{i\vec{k}\cdot(\vec{x}-\vec{z})}}{k^2}\, \bar{\psi}_a(\vec{x})\gamma_\mu \\ &\quad \times S_F(\vec{x},\vec{y};\epsilon_a - k_0)\gamma_\nu S_F(\vec{y},\vec{z};\epsilon_a - k_0)\gamma^\mu \psi_a(\vec{z})\bar{\psi}_v(\vec{w})\gamma^\nu \psi_v(\vec{w}), \qquad (31)\end{aligned}$$

$$\begin{aligned}\Delta E_4 &= 4i\pi\alpha^2 \sum_a \int d^3x\, d^3y\, d^3z\, d^3w\, \frac{e^{iE_{va}|\vec{y}-\vec{w}|}}{|\vec{y}-\vec{w}|} \int \frac{d^nk}{(2\pi)^n} \frac{e^{i\vec{k}\cdot(\vec{x}-\vec{z})}}{k^2}\, \bar{\psi}_a(\vec{x})\gamma_\mu \\ &\quad \times S_F(\vec{x},\vec{y};\epsilon_a - k_0)\gamma_\nu S_F(\vec{y},\vec{z};\epsilon_v - k_0)\gamma^\mu \psi_v(\vec{z})\bar{\psi}_v(\vec{w})\gamma^\nu \psi_a(\vec{w}), \qquad (32)\end{aligned}$$

$$\begin{aligned}\Delta E_5 &= -4i\pi\alpha \int d^3x\, d^3y\, d^3z \int \frac{d^nk}{(2\pi)^n} \frac{e^{i\vec{k}\cdot(\vec{x}-\vec{z})}}{k^2}\, \bar{\psi}_v(\vec{x})\gamma_\mu S_F(\vec{x},\vec{y};\epsilon_v - k_0)\gamma_0 \\ &\quad \times \tilde{U}(y)\, S_F(\vec{y},\vec{z};\epsilon_v - k_0)\gamma^\mu \psi_v(\vec{z}). \qquad (33)\end{aligned}$$

Here, ΔE_1 and ΔE_2 are the direct and exchange vertex terms of Fig. 4c for the valence electron while ΔE_3 and ΔE_4 are those for the core electron. As for ΔE_5, it is the counter-potential vertex term of Fig. 4d. We can combine ΔE_1 and ΔE_5 because angular momentum and parity selection rules restrict the value of ν to 0 in the former, which allows the d^3w integration and summation over a to be carried out, leading to the screening part of the core-Hartree potential, $U_{\rm CH}(y) - U_{\rm C}(y) = \alpha \int dy' \frac{1}{y_>}\rho_c(y')$, defined in Eq. (9). Rather than evaluate ΔE_1 and ΔE_5 separately, we instead treat their sum,

$$\begin{aligned}\Delta E_{15} &= 4i\pi\alpha \int d^3x\, d^3y\, d^3z \int \frac{d^nk}{(2\pi)^n}\, \frac{e^{i\vec{k}\cdot(\vec{x}-\vec{z})}}{k^2}\, \bar{\psi}_v(\vec{x})\gamma_\mu S_F(\vec{x},\vec{y};\epsilon_v - k_0)\gamma_0 \\ &\quad \times \Delta U(y) S_F(\vec{y},\vec{z};\epsilon_v - k_0)\gamma^\mu \psi_v(\vec{z}), \qquad (34)\end{aligned}$$

where $\Delta U \equiv U - U_{\rm CH} = U_{\rm KS} - U_{\rm CH}$ here. Note that had one used the core-Hartree potential, so that $U = U_{\rm CH}$, ΔE_{15} would vanish. Similar cancelations also take place between the valence-direct *side* term and the counter-potential *side* term arising from the first and

third terms in Eq. (25), as well as between the valence-direct and counter-potential terms in screened vacuum polarization calculations. The use of the core-Hartree potential thus simplifies the evaluation of screened Lamb shifts for alkalilike ions, a fact utilized by Blundell [25] in his QED calculations.

Besides combining ΔE_1 and ΔE_5 into ΔE_{15}, a further simplification occurs for the core-direct term ΔE_3 which, like the valence-direct term ΔE_1, can be shown to have only $\nu = 0$. In this case the core electron can be thought of as being *screened* by the valence electron with the potential

$$Y_{vv}(r) = \alpha \int dr' \, \frac{1}{r_>} [g_v(r')^2 + f_v(r')^2], \tag{35}$$

and we can write

$$\begin{aligned} \Delta E_3 \;=\; & -4i\pi\alpha \sum_a \int d^3x \, d^3y \, d^3z \int \frac{d^n k}{(2\pi)^n} \, \frac{e^{i\vec{k}\cdot(\vec{x}-\vec{z})}}{k^2} \, \bar{\psi}_a(\vec{x}) \gamma_\mu \\ & \times S_F(\vec{x}, \vec{y}; \epsilon_a - k_0) \gamma_0 Y_{vv}(y) S_F(\vec{y}, \vec{z}; \epsilon_a - k_0) \gamma^\mu \psi_a(\vec{z}). \end{aligned} \tag{36}$$

No simplifications are possible for the two exchange terms ΔE_2 and ΔE_4 outside of noting that they are equal to one another: their evaluation is the most challenging part of the screening calculation.

All of the above expressions are ultraviolet divergent as $n = 4 - \epsilon \to 4$, but the divergences arise only from terms in which both electron propagators are treated as free propagators. For this reason we begin by evaluating ΔE_i in this approximation, denoting such terms $\Delta E_i(0,0)$. It is possible to isolate the ultraviolet divergent part of these terms, which behave as $1/\epsilon$ and can be shown to exactly cancel the divergences arising from the derivative terms mentioned above. There remains the ultraviolet finite part of $\Delta E_i(0,0)$, which involves certain difficulties associated with the treatment of angular momentum and the fact that there are imaginary parts in the integrals, which are treated as described in Ref. [12].

We next form the ultraviolet finite combination $\Delta E_i - \Delta E_i(0,0)$ in coordinate space. As with the ladder and crossed-ladder diagrams, we first carry out a Wick rotation of the k_0 integration, $k_0 \to i\omega$, which passes a set of poles. The remaining integration over ω has the same singularities mentioned in connection with the derivative terms, and are regulated in the same manner. The sums of all the correction terms give the screened self-energy contributions, which are shown as "SE-screen" in Table I, along with the screened vacuum polarization contributions which are shown as "VP-screen".

V. RESIDUAL CORRECTIONS

A. Three photon effects

A QED treatment of three-photon effects is a large-scale task that has not yet been carried out. However, as discussed above, second-order MBPT roughly reproduces the full QED calculation. For this reason, to approximate three-photon effects we simply use third-order MBPT, including only the dominant Coulomb correction. An alternative approach would be to use configuration-interaction (CI) techniques which can give all-order results. To do this, one would have to carefully subtract out from the CI result the lowest-, first-, and second-order MBPT corrections using the same potential, and would then have a more complete treatment of higher-order corrections. However, because of the $1/Z$ expansion, these corrections are already quite small and this approach is not followed here.

B. Nuclear recoil

Recoil corrections arise from the small effect of the finite mass of the nucleus. For hydrogenic ions, while it suffices to simply use a reduced mass Rydberg constant as an overall scaling factor nonrelativistically, this is not valid when relativistic corrections are important. In the hydrogenic case, an exact treatment of terms first order in recoil leads to the formula [26]

$$\begin{aligned} E(n,j) \;=\; & mf(n,j) + \frac{m^2(Z\alpha)^2}{2Mn^2} + \frac{m^2(Z\alpha)^4}{M}\Big[-\frac{1}{2n^4} + \frac{1}{2n^3(j+1/2)}\Big] \\ & + \frac{m^2(Z\alpha)^5}{M} R(n,\kappa,Z\alpha), \end{aligned} \tag{37}$$

where $R(n,\kappa,Z\alpha)$ is given in Table III of Ref. [26] and

$$f(n,j) = \left\{1 + \frac{(Z\alpha)^2}{\Big[n-(j+1/2)+\sqrt{(j+1/2)^2-(Z\alpha)^2}\Big]^2}\right\}^{-1/2} \tag{38}$$

is the Dirac-Coulomb energy in units of mc^2. While we are dealing with lithiumlike ions, we make the approximation of using the recoil corrections in Eq. (37) for the $n = 2$ states considered here. To gauge the accuracy of doing this, we note that at $Z = 50$ the hydrogenic energy mf differs from the Kohn-Sham eigenvalues by only 5 percent. A comparable screening correction to the already small recoil term can definitely be ignored.

For many-electron systems such as the lithiumlike ions, there is an additional recoil term given by the expectation values of the operator

$$H_{\rm MP} = \frac{1}{2M} \sum_{i \neq j} \Big\{ \vec{p}_i \cdot \vec{p}_j + U(r_i) \Big[\vec{\alpha}_i + (\vec{\alpha}_i \cdot \hat{r}_i)\, \hat{r}_i \Big] \cdot \vec{p}_j \Big\}, \tag{39}$$

The first term in Eq. (39) is the mass polarization term and the second term is the leading relativistic correction [27]. The latter has been shown in Ref. [28] to arise from the exchange of one transverse photon in a QED formalism. The same work also showed that higher-order contributions from the exchange of two transverse photons, though extremely small at low Z, increase very rapidly along the isoelectronic sequence and are no longer negligible at high Z. Indeed, for the $2p_{1/2}$ state of hydrogenic uranium, contributions from the two terms in Eq. (39) give -0.085 and 0.068 eV for a sum of -0.017 eV, while the higher-order correction is comparable in size at -0.013 eV. Evaluations of these higher-order corrections with QED is non-trivial, but we find that they can be well approximated by the expectation values of the operator $\frac{1}{2M} \sum_{i \neq j} \vec{q}_i \cdot \vec{q}_j$ where

$$\vec{q}_i = \frac{1}{2}\, U(r_i) \Big[\vec{\alpha}_i + (\vec{\alpha}_i \cdot \hat{r}_i)\, \hat{r}_i \Big]. \tag{40}$$

Indeed, hydrogenic results thus obtained consistently agree with the QED results of [28] to within a few percent over a change of five orders of magnitude from $Z = 10$ to $Z = 100$. We thus use the operator

$$H^{\rm rel}_{\rm MP} = \frac{1}{2M} \sum_{i \neq j} \Big[\vec{p}_i \cdot \vec{p}_j + 2\, \vec{q}_i \cdot \vec{p}_j + \vec{q}_i \cdot \vec{q}_j \Big] \tag{41}$$

to evaluate the relativistic mass polarization corrections for lithiumlike ions with Kohn-Sham wave functions. Total recoil corrections as given by the sums of the hydrogenic mass correction factor and the expectation values of $H^{\rm rel}_{\rm MP}$ are tabulated as "Recoil" in Table I.

C. Two-loop Lamb shift

One of the major advances in QED bound state theory of recent years has been in the treatment of the two-loop Lamb shift. For hydrogen, this effect must be understood precisely before the proton size can be determined, and considerable effort had to be put into the $Z\alpha$ expansion of the effect before this could be done. As mentioned earlier, at high Z the effect, which in this case has to be calculated exactly without making the $Z\alpha$ expansion,

is large enough so that it could be clearly seen when comparing theory and experiment for lithiumlike bismuth [12]. In terms of a function $G(Z\alpha)$, the two-loop Lamb shift can be parameterized as

$$\Delta E_{2-\mathrm{loop}} = \frac{m\alpha^2}{\pi^2 n^3}(Z\alpha)^4 G(Z\alpha). \tag{42}$$

The exact calculation of $G(Z\alpha)$ is quite complicated, but enough Z values have been evaluated [13, 14] that an interpolation can be made, and the results are tabulated as "2-loop" in Table I.

D. Nuclear polarization

By far the largest uncertainty associated with the properties of the nucleus in a lithiumlike ion is the root-mean-square charge radius. We will discuss in the next section how the use of different values of this parameter lead to significant changes in the $2s$ energy. However, a smaller effect is beginning to become important as higher precisions are reached, which is the effect of the polarizability of the nucleus. This is a large effect in muonic atoms [29] and, while smaller, needs to be included for highly-charged heavy ions. The graphs involved are of the same form as the ladder and crossed ladder diagrams of Figs. 2d and 2e, with the bottom electron replaced with a nucleus that is understood to be in an excited state. This nuclear polarization effect from the collective nuclear excitations, including vibrations, rotations, and giant dipole resonances, has been studied by Plenum and Soff [15] for even isotopes of actinide nuclei. Results from that work are included in our ionization and transition energies for some of the high-Z ions, and are listed as "NucPol" in Table I.

VI. DISCUSSION AND CONCLUSION

As we have mentioned in the Introduction, most works on high-precision calculations of the energy levels of lithiumlike ions are based on the Hamiltonian approach for structure calculations, with QED corrections calculated separately. Examples are the relativistic many-body perturbation theory (RMBPT) calculations of Blundell [25] and the relativistic configuration-interaction (RCI) calculations of Chen *et al.* [30]. The works of the St. Petersburg group [11, 14, 31–33], on the other hand, should be comparable to the present S-matrix calculations, as both use similar QED-based approaches which treat electron cor-

relations and radiative corrections consistently and systematically according to the number of virtual photons exchanged between electrons. Comparing the present work with other calculations on different contributions to the ionization and transition energies can reveal QED effects on the structure energies not attainable in the Hamiltonian approach and show the importance of the rigorous treatments of screened QED corrections.

In Table III, the present structure and nuclear recoil energies for the $2s-2p$ transitions are presented. Also shown are the RMBPT energies of Blundell [25] which include some recoil corrections, and the structure energies of RCI [30] and the St. Petersburg group denoted by StPete [33]. Structure energies relative to the present results are shown in Figs. 5 and 6 for the $2s-2p_{1/2}$ and $2s-2p_{3/2}$ transitions, respectively. While all calculations agree at low Z, it can be seen that RMBPT and RCI energies deviate more and more from the present results as Z increases, demonstrating the importance of rigorous QED treatments in calculating correlation energies beyond the no-pair approximation. It is notable that the structure energies of the St. Petersburg group appear to scatter around our results and deviations can be as large as 0.7 eV at $Z = 90$. Apparently, these discrepancies are due mainly to the finite nuclear size effect from the use of different root-mean-square nuclear radii in the two calculations which affects the $2s$ states considerably more than the $2p_{1/2}$ and $2p_{3/2}$ states, hence the similar scattered patterns in Figs. 5 and 6. While we use nuclear radius parameters from the tabulation of Johnson and Soff [17] except for thorium ($Z = 90$) and uranium ($Z = 92$) which are derived from measurements [18, 19], recent works of the St. Petersburg group [14, 32, 33] use data from the tabulation of Anglei [34] except for $Z = 43$, 61, 85, 89, and 91 where data are not available and have to be taken from Johnson and Soff [17] instead. Unfortunately, nuclear sizes are somewhat uncertain, and the fact that they can lead to large, irregular discrepancies like those shown in Figs. 5 and 6 for high-Z lithiumlike ions can be seen in the $2s-2p_{1/2}$ structure energies of thorium which is listed in Table III as 309.78 eV from the St. Petersburg group's 2007 paper [33], but is given by 309.19 eV in their earlier 2001 paper [31] that is much closer to the present value of 309.13 eV. At close to 0.7 eV, this is an extremely large change. Fortunately, QED and other small corrections are not affected by these nuclear uncertainties. Also, the works of Blundell [25] and RCI [30] both use the same nuclear parameters as the present work. Otherwise, it will be very difficult, if not impossible, to draw any useful conclusions from those comparisons.

As for the recoil energies, our results shown in Table III are in very good agreement

with those of the St. Petersburg group for the $2s - 2p_{1/2}$ transition along the isoelectronic sequence [31]. Similar agreements are found for the $2s - 2p_{3/2}$ transition where such data are available for a few ions from the same group [14, 32, 33]. Recoil energies in Blundell and RCI are obtained approximately from the reduced mass and mass polarization corrections and differ slightly from the present results at high Z. For simplicity, recoil energies from other calculations are not shown here.

In Table IV, the present one-loop and two-loop QED energies are shown and are compared with results from other calculations. Here, Blundell's QED energies already include estimates of two-loop Lamb shift contributions, while those of RCI and the St. Petersburg group are screened one-loop results only. QED energies relative to the present results are shown in Figs. 7 and 8 for the $2s - 2p_{1/2}$ and $2s - 2p_{3/2}$ transitions, respectively. We note that QED calculations in RCI are similar to this work and start from the Kohn-Sham potential, but only at the one-photon level as discussed in Sec. III, and lack two-photon screening corrections as discussed in Sec. IV B. Blundell's QED calculations start from the core-Hartree potential and include some screening corrections, but the vertex exchange terms ΔE_2 and ΔE_4 in Eqs. (30) and (32) are not calculated. Because of these approximations, QED energies of Blundell and RCI tend to deviate more and more from the present results as Z increases. By contrast, QED energies from the St. Petersburg group are in very good agreement with our results along the isoelectronic sequence, as the screened QED diagrams are calculated correctly in both works. It is interesting to note that the relaxed QED energies from the RCI calculations of Cheng *et al.* [35] are in very good agreement with the present results at high Z. This method is relative simple in that relaxation corrections to the QED energies of the $2s - 2p$ transitions are obtained by using different Kohn-Sham potentials specific to the $2s$, $2p_{1/2}$, and $2p_{3/2}$ states to calculate the one-loop radiative corrections for the initial and final states. While it appears to give very good screened QED results, it is nevertheless an *ad hoc* method that may not be suitable for systematic, high-precision calculations.

In Table V, total transition energies are compared between theory and experiment. Results relative to the present ones are shown in Figs. 9 and 10 for the $2s-2p_{1/2}$ and $2s-2p_{3/2}$ transitions, respectively. Empirical results at low to mid Z come from NIST's online database of atomic spectra [36], with beam-foil measurements at $Z = 47$ [37], 50 and 54 [38]. At high Z, available experimental results are from electron beam ion trap (EBIT) measurements [5, 39–42]. In general, our results are in very good agreement with experiment, while those

of Blundell [25] and RCI [30] tend to deviate from our results and from experiment at high Z. For the $2s - 2p_{1/2}$ transition, St. Petersburg group's results differ from our results at high Z for two reasons. First of all, most of their total transition energies are from the 2001 paper [31] and do not include two-loop Lamb shift corrections. This leads to the sudden jump in their results from $Z = 90$ to 92, as the latter is from the 2006 paper [14] and does include the two-loop correction. Secondly, as we have pointed out earlier, their structure energies are different from ours because of the choices of nuclear radii. Should they use our nuclear radius at $Z = 92$, their result would be in much closer agreement with ours and with experiment. As for the $2s - 2p_{3/2}$ transition, there are only a few total transition energies from the St. Petersburg group and they all include two-loop corrections. At $Z = 83$ their result is in very good agreement with experiment, with our energy lower by about 0.08 eV. In this case, if we use their nuclear radius, our result will go up by about 0.04 eV, in closer agreement with their result and with experiment. Nevertheless, while we are not aware of any total $2s - 2p_{3/2}$ transition energy at $Z = 90$ from the St. Petersburg group, their structure energy is higher than ours by 0.7 eV as we have shown in Table III and Fig. 6. That will surely make the transition energy much higher than experiment and no other corrections can come close to compensate for such a big difference.

It is interesting to note that in Fig. 6, the RCI-relax energies [35] are seen to be in very good agreement with experiment. This is due mainly to the changes in the QED energies after the relaxation corrections are included, but that is not the entire reason. As we have pointed out in Sec. IV A, for the $2s - 2p_{3/2}$ transition at high Z, QED corrections to the structure energies from the correct treatment of the ladder and cross-ladder diagrams happen to be about the same size as the two-loop Lamb shifts but in opposite signs. Thus, the good agreement between RCI-relax and experiment is partly due to cancelation of errors, as neither corrections are included in those calculations.

There are other approaches that produce ionization and transition energies for the $n = 2$ states of lithiumlike ions. Complete tabulations along the isoelectronic sequences are available from Cheng *et al.* [43] and Kim *et al.* [44]. Both are multiconfiguration Dirac-Fock (MCDF) calculations that are not particularly accurate, though the latter does include correlation corrections as derived from RMBPT energies [2]. As for the QED corrections, the treatments in these early works are crude: Cheng *et al.* used estimated QED values based on Mohr's Coulombic results [45], while Kim *et al.* employed the *ad hoc* Welton's method

[46] for their calculations. Neither of these tabulations are at the same level of accuracies as the calculations mentioned here. To our knowledge, the only complete, high-precision QED treatment of the series is that given here.

As we have shown here, theory and experiment have reached a point where small corrections such as the two-loop Lamb shift and nuclear recoil can now be studied. On a more practical side, comparisons between theory and experiment on the transition energies of high-Z lithiumlike ions can also be used to check, or even deduce the radii of heavy nuclei with high precision. The next step for the lithium isoelectronic sequence will be quite challenging, both theoretically and experimentally. On the latter side, the achievement of sub-0.1 eV precision requires extraordinary care, and issues of fitting resonance curves and controlling systematics make getting another order of magnitude problematical. The very high precision achieved for copperlike tungsten [6], however, suggests that this problem may be overcome. If so, the challenge to theory is considerable. We have already shown that the treatment of recoil involves approximations that will require basic progress in bound state quantum field theory to remove. In addition, our treatment of the third- and higher-order photon diagrams has been extremely crude, involving only MBPT with Coulomb photons. If a QED approach is to be implemented, the correlation diagrams that give this third-order contribution should, in principle, be replaced with QED exchange diagrams involving three photons. In addition, the three-loop Lamb shift would have to be treated, along with screening corrections to the two-loop Lamb shift and two-photon screening corrections to the one-loop Lamb shift. Finally one must confront the fact that nuclear polarization effects will start to become important. As with many other situations in atomic physics, an interesting blend of advanced QED bound state theory, advances in experimental technique, and nuclear structure theory will be involved as the lithium isolectronic sequence is studied in future.

Acknowledgments

The work of J.S. was supported in part by NSF Grant No. PHY-0757125. The work of K.T.C. was performed under the auspices of the U.S. Department of Energy by Lawrence

Livermore National Laboratory under Contract DE-AC52-07NA27344.

[1] H.P. Kelly, Phys. Rev. **131**, 684 (1963).

[2] W.R. Johnson, S.A. Blundell, and J. Sapirstein, Phys. Rev. A **37**, 2764 (1988).

[3] W.R. Johnson, S.A. Blundell, and J. Sapirstein, Phys. Rev. A **38**, 2699 (1988).

[4] S.A. Blundell, Phys. Rev. A **46**, 3762 (1992); H. Persson, I. Lindgren, and S. Salomonson, Phys. Scr. T**46**, 125 (1993); K.T. Cheng, W.R. Johnson and J. Sapirstein, Phys. Rev. A **47**, 1817 (1993).

[5] P. Beiersdorfer, A.L. Osterheld, J.H. Scofield, J.R. Crespo Lopez-Urrutia, and K. Widmann, Phys. Rev. Lett. **80**, 3022 (1998).

[6] E. Lindroth, H. Danared, P. Glans, Z. Pesic, M. Tokman, G. Vikor, and R. Schuch, Phys. Rev. Lett. **86**, 5027 (2002).

[7] J.D. Gillaspy, I.N. Draganic, Yu. Ralchenko, J. Reader, J.N. Tan, J.M. Pomeroy, and S.M. Brewer, Phys. Rev. A **80**, 010501(R), 2009.

[8] J. Sucher, Int. J. Quantum Chem. **25**, 3 (1984).

[9] M. Mittleman, Phys. Rev. A **4**, 893 (1971); Phys. Rev. A **5**, 2395 (1972).

[10] J. Sucher, Phys. Rev. **107**, 1448 (1957).

[11] V.A. Yerokhin, A.N. Artemyev, T. Beier, G. Plunien, V.M. Shabaev, and G. Soff, Phys. Rev. A **60**, 3522 (1999).

[12] J. Sapirstein and K.T. Cheng, Phys. Rev. A **64**, 022502 (2001).

[13] V.A. Yerokhin, Phys. Rev. A **80**, 040501(R) (2009).

[14] V.A. Yerokhin, P. Indelicato, and V.M. Shabaev, Phys. Rev. Lett. **97**, 253044 (2006).

[15] G. Plunien and G. Soff, Phys. Rev. A **51**, 1119 (1995). Due to a mistake in the formulas, results of this work are too large by a factor of 2π as pointed out in the erratum: G. Plunien and G. Soff, Phys. Rev. A **53**, 4614 (1996).

[16] R. Cowan, *The Theory of Atomic Spectra*, Chapter 7, Section 7-11.

[17] W.R. Johnson and G. Soff, At. Data Nuc. Data Tables **33**, 405 (1985).

[18] J. D. Zumbro, R. A. Naumann, M. V. Hoehn, E. B. Shera, C. E. Bemis, Jr., and Y. Tanaka, Phys. Lett. **167B**, 383 (1986).

[19] J. D. Zumbro, E. B. Shera, Y. Tanaka, C. E. Bemis, Jr., R. A. Naumann, M. V. Hoehn, W.

Reuter, and R. M. Steffen, Phys. Rev. Lett. **53**, 1888 (1984).

[20] W.H. Furry, Phys. Rev. **81**, 115 (1951).

[21] E.H. Wichmann and N.M. Kroll, Phys. Rev. **101**, 843 (1956).

[22] J. Sapirstein and K.T. Cheng, Phys. Rev. A **68**, 042111 (2003).

[23] J. Sapirstein and K.T. Cheng, Phys. Rev. A **73**, 012503 (2006).

[24] P.J. Mohr and J. Sapirstein, Phys. Rev. A **62**, 052501 (2000).

[25] S.A. Blundell, Phys. Rev. A **47**, 1790 (1993).

[26] G.A. Adkins, S. Morrison, and J. Sapirstein, Phys. Rev. A **76**, 042508 (2007).

[27] C.W.P. Palmer, J. Phys. B **20**, 5987 (1987); A.P. Stone, Proc. Phys. Soc. **77**, 786 (1961); *ibid* **81** 868 (1963).

[28] A.N. Artemyev, V.M. Shabaev and V.A. Yerokhin, Phys. Rev. A **52**, 1884 (1995).

[29] E. Borie and G.A. Rinker, Rev. Mod. Phys. 54, 67 (1982).

[30] M.H. Chen, K.T. Cheng, W.R. Johnson, and J. Sapirstein, Phys. Rev. A **52**, 266 (1995).

[31] V.A. Yerokhin, A.N. Artemyev, V.M. Shabaev, M.M Sysak, O.M Zherebtsov, and G. Soff, Phys. Rev. A **64**, 032109 (2001).

[32] Y.S. Kozhedub, D.A. Glazov, A.N. Artemyev, N.S. Oreshkina, V.M. Shabaev, I.I. Tupitsyn, A.V. Volotka, and G. Plunien, Phys. Rev. A **75**, 062501 (2007).

[33] V.A. Yerokhin, A.N. Artemyev, and V.M. Shabaev, Phys. Rev. A **75**, 062501 (2007).

[34] I. Angeli, At. Data Nuc. Data Tables **87**, 185 (2004).

[35] K.T. Cheng, M.H.Chen, and J. Sapirstein, Phys. Rev. A **62**, 054501 (2000).

[36] NIST Atomic Spectra Database, http://physics.nist.gov/PhysRefData/ASD.

[37] Ph. Bosselmann, U. Staude, D. Horn, K.-H. Schartner, F. Folkmann, A. E. Livingston, and P. H. Mokler, Phys. Rev. A **59**, 1874 (1999).

[38] D. Feili, Ph. Bosselmann, K.-H. Schartner, F. Folkmann, A. E. Livingston, E. Träbert, X. Ma, and P. H. Mokler, Phys. Rev. A **62**, 022501 (2000).

[39] X. Zhang, N. Nakamura, C. Chen, M. Andersson, Y. Liu, and S. Ohtani, Phys. Rev. A **78**, 032504 (2008).

[40] P. Beiersdorfer, A. Osterheld, S.R. Elliott, M.H. Chen, D. Knapp, and K. Reed, Phys. Rev. A **52**, 2693 (1995).

[41] P. Beiersdorfer, H. Chen, D.B. Thorn, and E. Träbert, Phys. Rev. Lett **95**, 233003 (2005).

[42] P. Beiersdorfer, D. Knapp, R.E. Marrs, S.R. Elliot, and M.H. Chen, Phys. Rev. Lett. **71**, 3939

(1993); P. Beiersdorfer, Nucl. Instrum. Methods Phys. Res. B **99**, 114 (1995).

[43] K.T. Cheng, Y.-K. Kim, and J.P. Desclaux, At. Data Nuc. Data Tables **24**, 111 (1979).

[44] Y.-K. Kim, D.H. Baik, P. Indelicato, and J.P. Desclaux, Phys. Rev. A **44**, 148 (1991).

[45] P. Mohr, Ann. Phys. (N.Y.) **88**, 26 (1974); *ibid* **88**, 52 (1974).

[46] T.A. Welton, Phys. Rev. **74**, 1157 (1948).

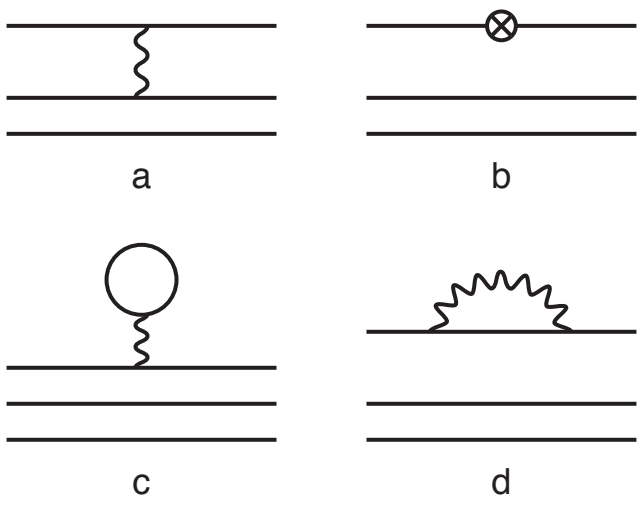

FIG. 1: One-photon correlation and radiative diagrams. A cross inside a circle represents a counter-potential.

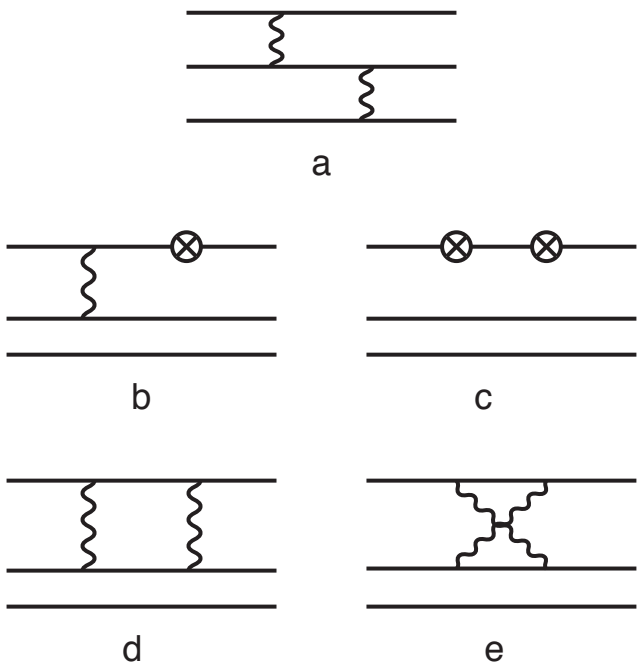

FIG. 2: Two-photon correlation diagrams. A cross inside a circle represents a counter-potential.

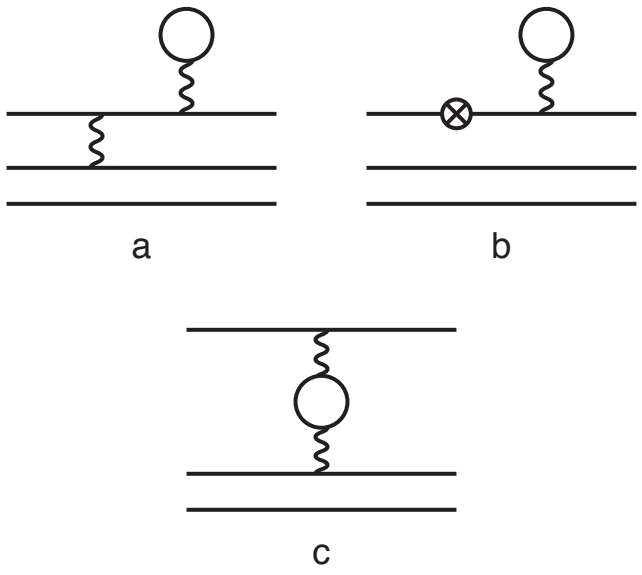

FIG. 3: Screened vacuum polarization diagrams. A cross inside a circle represents a counter-potential.

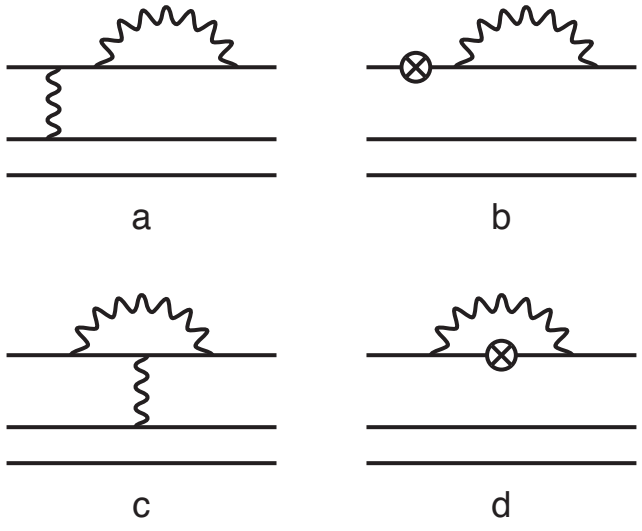

FIG. 4: Screened self-energy diagrams. A cross inside a circle represents a counter-potential.

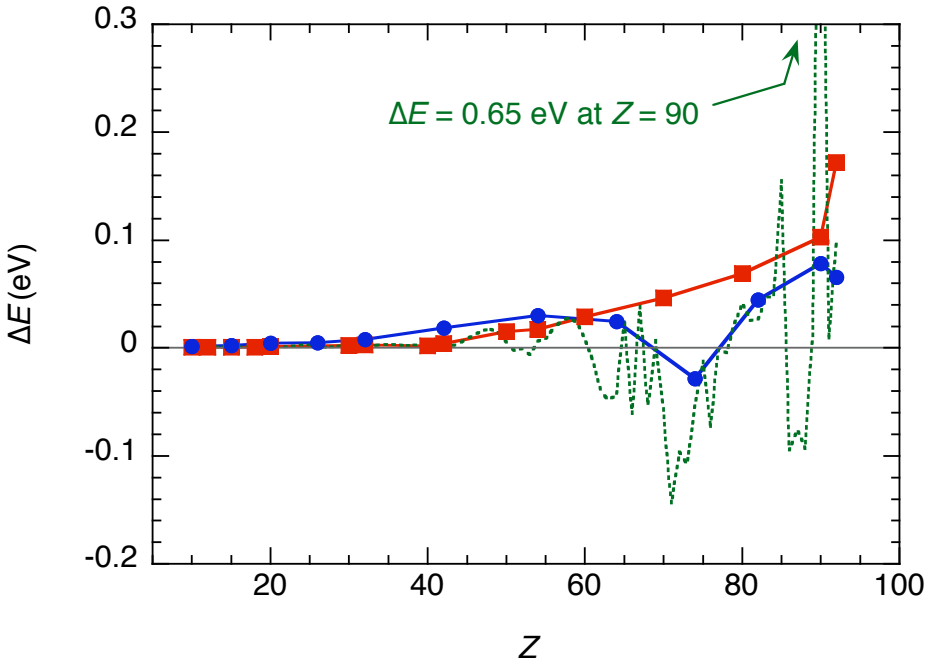

FIG. 5: Structure energies (eV) of the $2s - 2p_{1/2}$ transition relative to the present results. Solid rectangles: Blundell [25]. Solid circles: RCI [30]. Dotted line: St. Petersburg group [33].

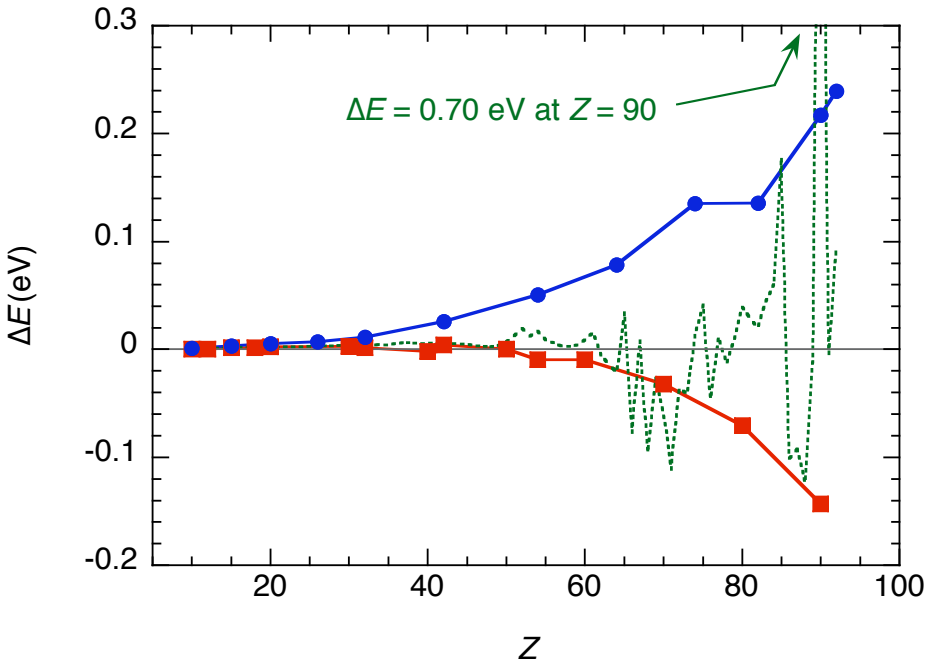

FIG. 6: Structure energies (eV) of the $2s - 2p_{3/2}$ transition relative to the present results. Solid rectangles: Blundell [25]. Solid circles: RCI [30]. Dotted line: St. Petersburg group [33].

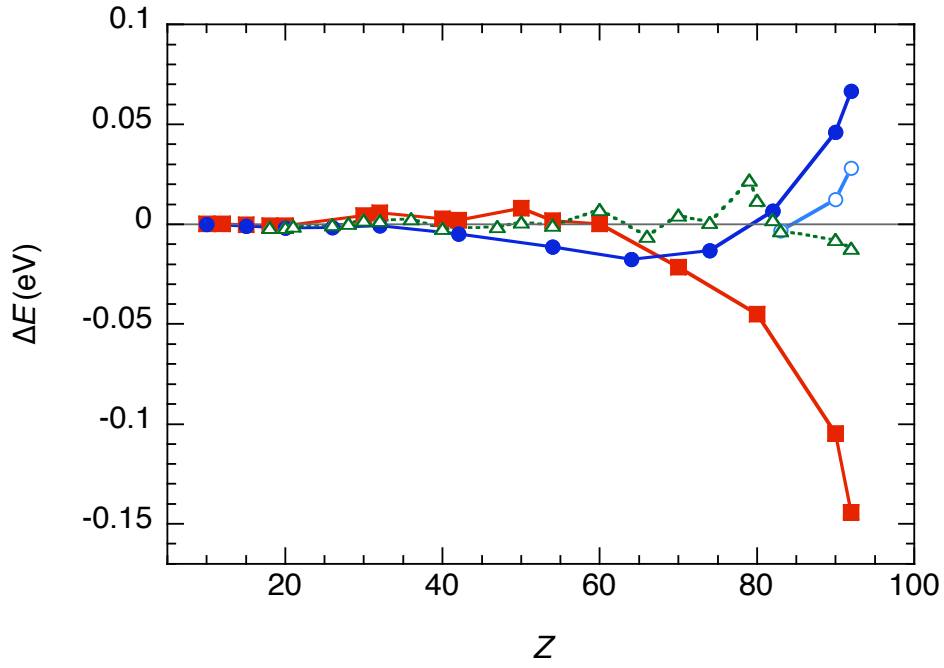

FIG. 7: Screened QED energies (eV) of the $2s - 2p_{1/2}$ transition relative to the present results. Solid rectangles: Blundell. Solid circles: RCI. Open circles: RCI relaxed QED. Open triangles: St. Petersburg group. See Table IV for references.

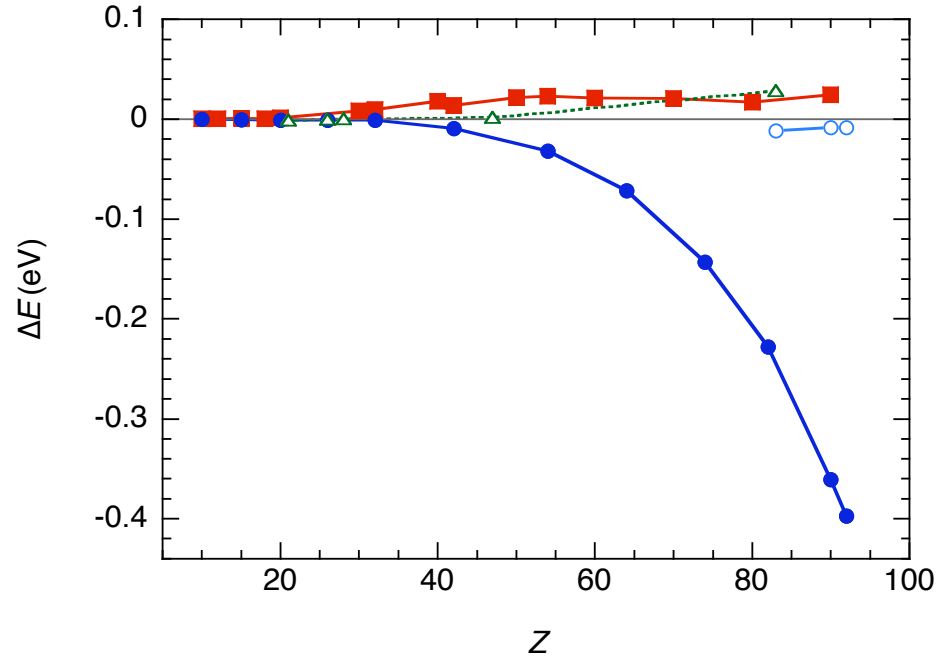

FIG. 8: Screened QED energies (eV) of the $2s - 2p_{3/2}$ transition relative to the present results. Solid rectangles: Blundell. Solid circles: RCI. Open circles: RCI relaxed QED. Open triangles: St. Petersburg group. See Table IV for references.

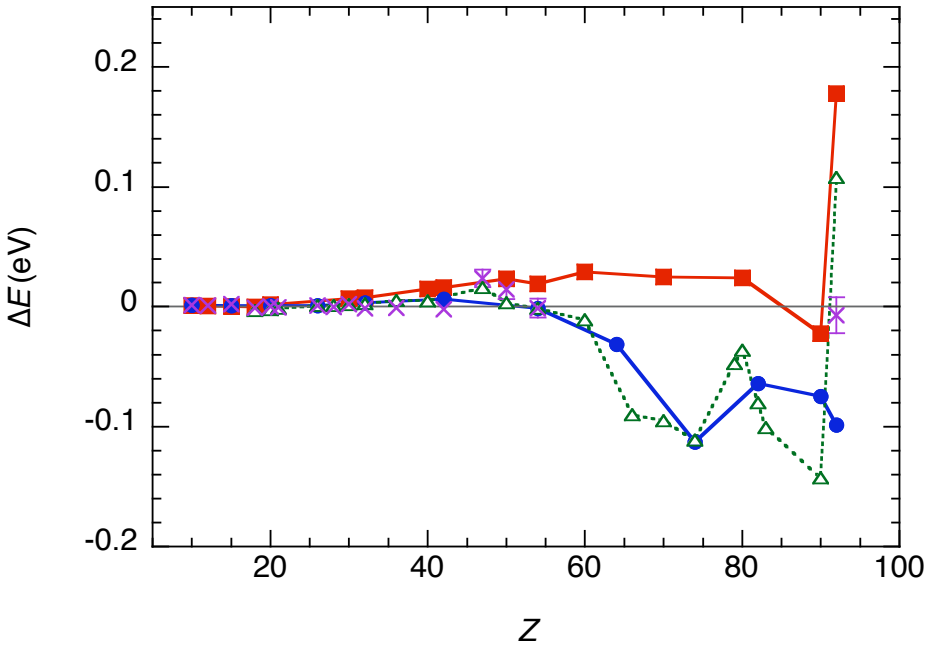

FIG. 9: The $2s - 2p_{1/2}$ transition energies (eV) relative to the present results. Solid rectangles: Blundell. Solid circles: RCI. Open triangles: St. Petersburg group. Crosses: Experiment. See Table V for references.

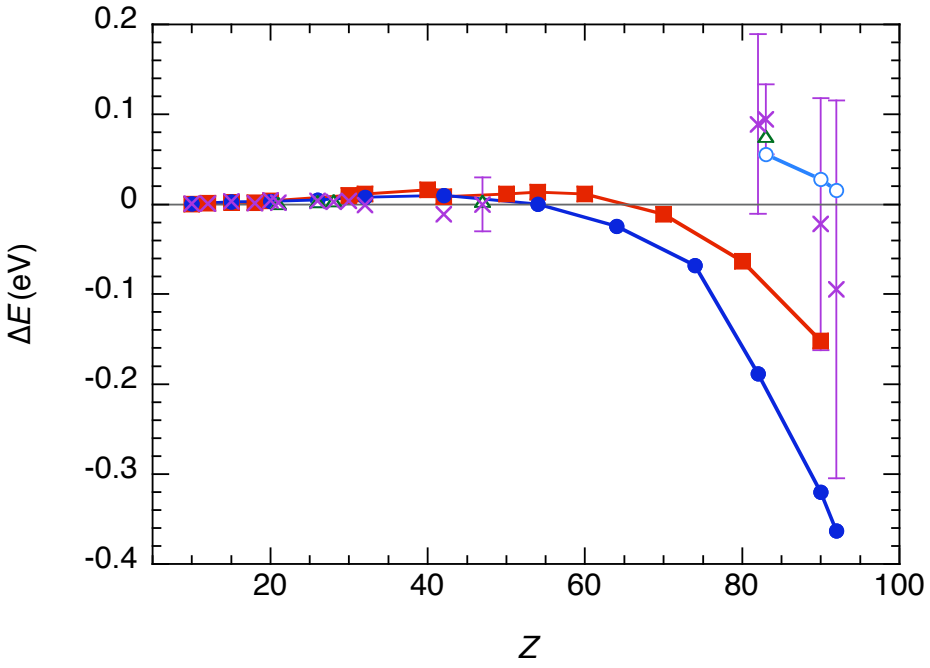

FIG. 10: The $2s - 2p_{3/2}$ transition energies (eV) relative to the present results. Solid rectangles: Blundell. Solid circles: RCI. Open circles: RCI with relaxed QED. Open triangles: St. Petersburg group. Crosses: Experiment. See Table V for references.

TABLE I: Breakdown of contributions to the ionization potentials (a.u.) for the $n = 2$ states of selected lithiumlike ions. See text for term notations.

State	Terms	$Z = 20$	$Z = 40$	$Z = 60$	$Z = 74$	$Z = 83$	$Z = 92$
$2s_{1/2}$	$E^{(0)}$	-41.07821	-186.1698	-449.2213	-718.3888	-937.4309	-1201.067
	$E^{(1)}$	-1.47173	-3.0515	-4.6537	-5.8045	-6.5674	-7.360
	$E^{(2)}$	-0.00344	-0.0057	-0.0098	-0.0141	-0.0178	-0.023
	$E^{(3)}$	-0.00002	0.0000	0.0000	0.0000	0.0000	0.000
	Recoil	0.00069	0.0013	0.0020	0.0027	0.0035	0.005
	Uehling	-0.00052	-0.0094	-0.0579	-0.1656	-0.3123	-0.582
	WK	0.00000	0.0001	0.0015	0.0060	0.0136	0.029
	SE	0.00729	0.0896	0.3967	0.9017	1.4586	2.314
	VP-screen	0.00003	0.0003	0.0013	0.0033	0.0060	0.011
	SE-screen	-0.00030	-0.0020	-0.0070	-0.0147	-0.0233	-0.037
	2-loop	-0.00001	-0.0002	-0.0009	-0.0026	-0.0046	-0.008
	NucPol						-0.001
	Sum	-42.54621	-189.1475	-453.5492	-723.4766	-942.8748	-1206.719
$2p_{1/2}$	$E^{(0)}$	-39.78590	-183.3083	-444.4356	-711.9216	-929.7361	-1192.233
	$E^{(1)}$	-1.43120	-2.8467	-3.9741	-4.4418	-4.5141	-4.305
	$E^{(2)}$	-0.00743	-0.0122	-0.0226	-0.0364	-0.0502	-0.070
	$E^{(3)}$	0.00007	0.0000	0.0001	0.0001	0.0001	0.000
	Recoil	0.00033	0.0006	0.0009	0.0012	0.0016	0.002
	Uehling	0.00000	-0.0002	-0.0033	-0.0157	-0.0399	-0.098
	WK	0.00000	0.0000	0.0001	0.0008	0.0025	0.007
	SE	-0.00022	-0.0014	0.0086	0.0570	0.1422	0.321
	VP-screen	0.00003	0.0003	0.0012	0.0032	0.0060	0.012
	SE-screen	-0.00030	-0.0020	-0.0067	-0.0147	-0.0243	-0.041
	2-loop	0.00000	0.0000	0.0001	0.0001	0.0001	0.000
	NucPol						0.000
	Sum	-41.22462	-186.1698	-448.4315	-716.3678	-934.2122	-1196.406
$2p_{3/2}$	$E^{(0)}$	-39.58248	-179.3907	-422.1043	-655.2997	-833.7473	-1035.279
	$E^{(1)}$	-1.44944	-3.0233	-4.6710	-5.9317	-6.8275	-7.830
	$E^{(2)}$	-0.00697	-0.0093	-0.0124	-0.0146	-0.0159	-0.017
	$E^{(3)}$	0.00006	0.0000	0.0000	0.0000	0.0000	0.000
	Recoil	0.00033	0.0005	0.0008	0.0010	0.0011	0.001
	Uehling	0.00000	0.0000	-0.0003	-0.0010	-0.0021	-0.004
	WK	0.00000	0.0000	0.0000	0.0001	0.0003	0.001
	SE	0.00020	0.0059	0.0395	0.1070	0.1852	0.303
	VP-screen	0.00003	0.0002	0.0008	0.0016	0.0025	0.004
	SE-screen	-0.00033	-0.0019	-0.0052	-0.0089	-0.0120	-0.016
	2-loop	0.00000	0.0000	0.0000	-0.0001	-0.0002	-0.001
	NucPol						0.000
	Sum	-41.03860	-182.4185	-426.7520	-661.1463	-840.4160	-1042.837

TABLE II: Ionization potentials (a.u.) and transition energies (eV) for the $n = 2$ states of lithium-like ions.

Z	$2s$	$2p_{1/2}$	$2p_{3/2}$	$2s - 2p_{1/2}$	$2s - 2p_{3/2}$	Z	$2s$	$2p_{1/2}$	$2p_{3/2}$	$2s - 2p_{1/2}$	$2s - 2p_{3/2}$
10	-8.786573	-8.202716	-8.195174	15.8876	16.0928	56	-390.1477	-385.5147	-369.4820	126.069	562.342
11	-11.01975	-10.36338	-10.35140	17.8606	18.1867	57	-405.4716	-400.7209	-383.4008	129.272	600.577
12	-13.50530	-12.77626	-12.75813	19.8382	20.3315	58	-421.1434	-416.2728	-397.5850	132.534	641.057
13	-16.24373	-15.44179	-15.41539	21.8219	22.5403	59	-437.1677	-432.1748	-412.0351	135.863	683.892
14	-19.23555	-18.36047	-18.32322	23.8123	24.8258	60	-453.5492	-448.4315	-426.7520	139.261	729.189
15	-22.48144	-21.53287	-21.48176	25.8118	27.2026	61	-470.2924	-465.0478	-441.7361	142.713	777.058
16	-25.98197	-24.95961	-24.89107	27.8198	29.6850	62	-487.4023	-482.0293	-456.9878	146.206	827.621
17	-29.73794	-28.64142	-28.55128	29.8380	32.2907	63	-504.8851	-499.3811	-472.5078	149.772	881.033
18	-33.75011	-32.57898	-32.46252	31.8681	35.0371	64	-522.7451	-517.1085	-488.2968	153.379	937.386
19	-38.01921	-36.77309	-36.62490	33.9086	37.9411	65	-540.9890	-535.2170	-504.3554	157.063	996.849
20	-42.54621	-41.22462	-41.03860	35.9623	41.0242	66	-559.6227	-553.7123	-520.6846	160.830	1059.56
21	-47.33211	-45.93451	-45.70381	38.0308	44.3084	67	-578.6484	-572.6002	-537.2850	164.579	1125.56
22	-52.37781	-50.90371	-50.62065	40.1124	47.8148	68	-598.0810	-591.8871	-554.1573	168.545	1195.23
23	-57.68441	-56.13326	-55.78933	42.2089	51.5677	69	-617.9178	-611.5790	-571.3025	172.486	1268.47
24	-63.25298	-61.62422	-61.21002	44.3209	55.5918	70	-638.1702	-631.6827	-588.7214	176.535	1345.57
25	-69.08477	-67.37775	-66.88297	46.4505	59.9142	71	-658.8459	-652.2056	-606.4146	180.693	1426.73
26	-75.18098	-73.39500	-72.80837	48.5989	64.5620	72	-679.9497	-673.1556	-624.3826	184.876	1512.06
27	-81.54295	-79.67733	-78.98646	50.7662	69.5656	73	-701.4919	-694.5404	-642.6262	189.159	1601.82
28	-88.17198	-86.22608	-85.41744	52.9507	74.9548	74	-723.4766	-716.3678	-661.1463	193.441	1696.10
29	-95.06961	-93.04267	-92.10162	55.1558	80.7632	75	-745.9182	-738.6462	-679.9436	197.881	1795.26
30	-102.2373	-100.1285	-99.03921	57.3821	87.0231	76	-768.8199	-761.3839	-699.0192	202.345	1899.37
31	-109.6765	-107.4851	-106.2305	59.6316	93.7714	77	-792.1926	-784.5898	-718.3739	206.882	2008.71
32	-117.3890	-115.1141	-113.6758	61.9035	101.044	78	-816.0463	-808.2734	-738.0087	211.510	2123.51
33	-125.3765	-123.0172	-121.3753	64.1994	108.879	79	-840.3900	-832.4441	-757.9245	216.218	2244.00
34	-133.6408	-131.1962	-129.3294	66.5196	117.317	80	-865.2323	-857.1120	-778.1223	220.966	2370.38
35	-142.1836	-139.6528	-137.5384	68.8659	126.401	81	-890.5884	-882.2884	-798.6029	225.855	2503.05
36	-151.0070	-148.3890	-146.0027	71.2399	136.174	82	-916.4651	-907.9848	-819.3671	230.760	2642.17
37	-160.1129	-157.4066	-154.7224	73.6423	146.682	83	-942.8748	-934.2122	-840.4160	235.721	2788.04
38	-169.5035	-166.7079	-163.6981	76.0731	157.974	84	-969.8326	-960.9831	-861.7507	240.806	2941.06
39	-179.1809	-176.2949	-172.9300	78.5335	170.097	85	-997.3441	-988.3106	-883.3720	245.814	3101.34
40	-189.1475	-186.1698	-182.4185	81.0253	183.104	86	-1025.424	-1016.208	-905.2811	250.776	3269.26
41	-199.4054	-196.3351	-192.1641	83.5488	197.047	87	-1054.097	-1044.691	-927.4787	255.954	3445.45
42	-209.9572	-206.7929	-202.1670	86.1041	211.982	88	-1083.366	-1073.772	-949.9662	261.083	3630.00
43	-220.8055	-217.5459	-212.4277	88.6964	227.969	89	-1113.254	-1103.467	-972.7445	266.311	3823.46
44	-231.9527	-228.5967	-222.9467	91.3199	245.066	90	-1143.741	-1133.791	-995.8155	270.743	4025.25
45	-243.4017	-239.9480	-233.7242	93.9791	263.338	91	-1174.936	-1164.768	-1019.179	276.669	4238.37
46	-255.1554	-251.6026	-244.7608	96.6765	282.849	92	-1206.719	-1196.406	-1042.837	280.652	4459.46
47	-267.2166	-263.5631	-256.0570	99.4141	303.667	93	-1239.273	-1228.736	-1066.790	286.708	4693.50
48	-279.5882	-275.8327	-267.6132	102.192	325.858	94	-1272.477	-1261.769	-1091.040	291.376	4937.14
49	-292.2738	-288.4144	-279.4299	105.020	349.502	95	-1306.418	-1295.529	-1115.588	296.308	5192.76
50	-305.2764	-301.3113	-291.5076	107.897	374.668	96	-1341.095	-1330.038	-1140.435	300.890	5460.25
51	-318.5993	-314.5269	-303.8468	110.816	401.436	97	-1376.544	-1365.321	-1165.582	305.400	5740.56
52	-332.2459	-328.0650	-316.4479	113.769	429.885	98	-1412.778	-1401.403	-1191.031	309.526	6034.05
53	-346.2207	-341.9290	-329.3114	116.781	460.124	99	-1449.814	-1438.309	-1216.782	313.055	6341.12
54	-360.5261	-356.1228	-342.4379	119.821	492.206	100	-1487.696	-1476.073	-1242.837	316.288	6662.94
55	-375.1674	-370.6500	-355.8279	122.923	526.255						

TABLE III: The present structure and recoil energies (eV) for the $2s-2p$ transitions of lithiumlike ions are compared with other theoretical results. Blundell's RMBPT energies [25] already include recoil corrections. RCI [30] and St. Petersburg group's results StPete [33] are structure energies only.

	$2s-2p_{1/2}$					$2s-2p_{3/2}$				
Z	Structure	Recoil	Blundell	RCI	StPete	Structure	Recoil	Blundell	RCI	StPete
10	15.906	-0.004	15.903	15.907	15.906	16.110	-0.004	16.107	16.111	16.110
12	19.872	-0.005	19.867		19.872	20.364	-0.005	20.359		20.364
15	25.884	-0.006	25.878	25.886	25.885	27.272	-0.007	27.267	27.275	27.273
18	32.005	-0.008	31.998		32.006	35.167	-0.008	35.161		35.169
20	36.162	-0.010	36.154	36.167	36.163	41.213	-0.010	41.206	41.218	41.215
21	38.267	-0.009			38.268	44.532	-0.010			44.534
26	49.101	-0.012		49.106	49.103	65.030	-0.012		65.037	65.033
28	53.603	-0.014			53.603	75.560	-0.014			75.563
30	58.211	-0.014	58.199		58.213	87.789	-0.015	87.777		87.793
32	62.940	-0.014	62.928	62.948	62.942	102.00	-0.015	101.98	102.01	102.00
36	72.798	-0.016			72.801	137.60	-0.017			137.60
40	83.267	-0.019	83.250		83.270	185.14	-0.020	185.12		185.15
42	88.755	-0.019	88.740	88.774	88.759	214.39	-0.021	214.37	214.41	214.39
47	103.33	-0.023			103.34	307.20	-0.024			307.20
50	112.74	-0.023	112.73		112.74	379.03	-0.025	379.00		379.03
54	126.14	-0.025	126.13	126.17	126.14	497.88	-0.028	497.84	497.93	497.89
60	148.37	-0.030	148.37		148.38	737.35	-0.033	737.31		737.36
64	164.79	-0.032		164.81	164.74	947.61	-0.036		947.69	947.59
66	173.54	-0.033			173.47	1070.96	-0.038			1070.88
70	192.16	-0.036	192.17		192.10	1359.62	-0.042	1359.55		1359.56
74	212.46	-0.040		212.43	212.41	1713.27	-0.048		1713.40	1713.28
79	240.24	-0.046			240.26	2265.85	-0.056			2265.86
80	246.09	-0.047	246.11		246.13	2393.28	-0.057	2393.15		2393.32
82	258.20	-0.050		258.25	258.23	2667.29	-0.061		2667.43	2667.31
83	264.38	-0.052			264.43	2814.35	-0.064			2814.39
90	309.13	-0.065	309.17	309.21	309.78	4061.21	-0.084	4060.98	4061.42	4061.91
92	322.23	-0.071	322.33	322.29	322.33	4498.69	-0.092		4498.93	4498.79

TABLE IV: The present screened 1-loop and 2-loop QED energies (eV) for the $2s-2p$ transitions of lithiumlike ions are compared with other theoretical results. Blundell's results are from [25], RCI and RCI-relax results are from [30] and [35], respectively, and St. Petersburg group's results StPete are from [31] unless otherwise specified. While Blundell includes estimates of higher-order corrections, others are screened 1-loop results only.

	$2s-2p_{1/2}$						$2s-2p_{3/2}$					
Z	1-loop	2-loop	Blundell	RCI	RCI-relax	StPete	1-loop	2-loop	Blundell	RCI	RCI-relax	StPete
10	-0.014	0.000	-0.014	-0.014			-0.014	0.000	-0.014	-0.014		
12	-0.029	0.000	-0.028				-0.028	0.000	-0.027			
15	-0.066	0.000	-0.066	-0.067			-0.063	0.000	-0.062	-0.063		
18	-0.129	0.000	-0.130			-0.131	-0.123	0.000	-0.122			
20	-0.190	0.000	-0.191	-0.192		-0.192	-0.180	0.000	-0.178	-0.181		
21	-0.228	0.000				-0.229[a]	-0.214	0.000				-0.215[a]
26	-0.491	0.001		-0.493		-0.492[b]	-0.457	0.001		-0.458		-0.457[b]
28	-0.639	0.001				-0.639[b]	-0.592	0.001				-0.592[b]
30	-0.816	0.002	-0.810			-0.814	-0.753	0.002	-0.743			
32	-1.024	0.002	-1.016	-1.025		-1.022	-0.941	0.002	-0.929	-0.942		
36	-1.545	0.004				-1.543[b]	-1.411	0.003				
40	-2.228	0.005	-2.220			-2.230	-2.023	0.005	-2.000			
42	-2.638	0.007	-2.630	-2.643			-2.390	0.006	-2.370	-2.400		
47	-3.899	0.010				-3.900	-3.514	0.010				-3.512[b]
50	-4.831	0.013	-4.810			-4.830	-4.344	0.012	-4.310			
54	-6.309	0.018	-6.290	-6.321		-6.310	-5.660	0.017	-5.620	-5.692		
60	-9.107	0.027	-9.080			-9.100	-8.157	0.025	-8.110			
64	-11.41	0.037		-11.43			-10.22	0.034		-10.30		
66	-12.71	0.042				-12.72	-11.40	0.039				
70	-15.64	0.056	-15.61			-15.64	-14.06	0.051	-13.99			
74	-19.05	0.073		-19.06		-19.05	-17.19	0.067		-17.33		
79	-24.07	0.101				-24.05	-21.88	0.093				
80	-25.18	0.107	-25.12			-25.17	-22.94	0.099	-22.82			
82	-27.51	0.121		-27.51		-27.51	-25.17	0.112		-25.40		
83	-28.74	0.129			-28.74	-28.74	-26.36	0.120			-26.37	-26.33[c]
90	-38.54	0.197	-38.45	-38.50	-38.53	-38.55	-36.08	0.187	-35.87	-36.44	-36.09	
92	-41.76	0.222	-41.68	-41.69	-41.73	-41.77[c]	-39.38	0.212		-39.78	-39.39	

[a]Ref. [32].
[b]Ref. [33].
[c]Ref. [14].

TABLE V: The $2s - 2p$ transition energies (eV) of lithiumlike ions. Blundell's results are from [25]. Unless otherwise specified, RCI results are from [30], St. Petersburg group's results StPete are from [31], and experimental results are from the NIST Atomic Spectra Database [36].

	$2s - 2p_{1/2}$					$2s - 2p_{3/2}$				
Z	Present	Blundell	RCI	StPete	Expt	Present	Blundell	RCI	StPete	Expt
10	15.888	15.889	15.889		15.88881	16.093	16.093	16.093		16.09330
12	19.838	19.839			19.8393	20.331	20.332			20.3320
15	25.812	25.812	25.813		25.8140	27.203	27.205	27.205		27.206
18	31.868	31.868		31.865	31.8672	35.037	35.039			35.0383
20	35.962	35.964	35.963	35.960	35.9625	41.024	41.028	41.028		41.0286
21	38.031			38.029[a]	38.03	44.308			44.309[a]	44.31
26	48.599		48.600	48.600[b]	48.5997	64.562		64.567	64.565[b]	64.5656
28	52.951			52.952[b]	52.9503	74.955			74.959[b]	74.9574
30	57.382	57.389		57.384	57.3843	87.023	87.033			87.0272
32	61.904	61.911	61.907	61.906	61.9023	101.04	101.06	101.05		101.043
36	71.240			71.245[b]	71.2391	136.17				
40	81.025	81.040		81.030		183.10	183.12			
42	86.104	86.120	86.110		86.1021	211.98	211.99	211.99		211.9706
47	99.414			99.430	99.438[c]	303.67			303.67[b]	303.67[c]
50	107.90	107.92		107.90	107.91[d]	374.67	374.68			
54	119.82	119.84	119.82	119.82	119.82[d]	492.21	492.22	492.21		
60	139.26	139.29		139.25		729.19	729.20			
64	153.38		153.35			937.39		937.36		
66	160.83			160.74		1059.56				
70	176.54	176.56		176.44		1345.57	1345.56			
74	193.44		193.33	193.33		1696.10		1696.03		
79	216.22			216.17		2244.00				
80	220.97	220.99		220.93		2370.38	2370.32			
82	230.76		230.70	230.68		2642.17		2641.98		2642.26[e]
83	235.72			235.62		2788.04		2788.10[f]	2788.12[g]	2788.139[h]
90	270.74[i]	270.72	270.67	270.60		4025.25[j]	4025.10	4025.28[f]		4025.23[k]
92	280.65[i]	280.83	280.55	280.76[g]	280.645[l]	4459.46[j]		4459.48[f]		4459.37[m]

[a]Ref. [32].
[b]Ref. [33].
[c]Beam-foil, Ref. [37].
[d]Beam-foil, Ref. [38].
[e]EBIT 2008, Ref. [39].
[f]RCI with relaxed QED corrections, Ref. [35].
[g]Ref. [14].
[h]EBIT, Ref. [5].
[i]Include nuclear polarization corrections of 0.21 eV for $Z = 90$ and 0.30 eV for $Z = 92$.
[j]Include nuclear polarization corrections of 0.23 eV for $Z = 90$ and 0.34 eV for $Z = 92$.
[k]EBIT, Ref. [40].
[l]EBIT, Ref. [41].
[m]EBIT, Ref. [42].